Microporous and Mesoporous Materials 204 (2015) 180–189

Contents lists available at ScienceDirect

Microporous and Mesoporous Materials

journal homepage: www.elsevier.com/locate/micromeso

Dehydration of glycerol to acrolein using H-ZSM5 zeolite modified by alkali treatment with NaOH

H.P. Decolatti, B.O. Dalla Costa, C.A. Querini *

Research Institute on Catalysis and Petrochemistry – INCAPE (UNL–CONICET), Santiago del Estero 2654, Santa Fe S3000AOJ, Argentina

ARTICLE INFO

Article history:
Received 25 September 2014
Received in revised form 10 November 2014
Accepted 17 November 2014
Available online 25 November 2014

Keywords:
Glycerol dehydration
Acrolein
ZSM5
Alkali treatment

ABSTRACT

The dehydration of glycerol to acrolein has been studied using H-ZSM5 zeolite treated in alkaline medium in order to develop mesoporosity by desilication. Treatment of H-ZSM5 zeolite (Si/Al: 15) in NaOH solutions leads to mesoporosity development due to the preferential extraction of Si from the zeolite framework (desilication) without significant modification of the intrinsic zeolite properties. The samples were studied by powder X-ray diffraction (XRD), N_2 adsorption, pyridine-temperature programmed desorption (Py-TPD) and FTIR of adsorbed pyridine. The coke deposits were analyzed by temperature programmed oxidation (TPO). The alkaline treatment conditions led to an increase in the mesopore surface area from 254 $m^2\ g^{-1}$ for the calcined zeolite to 325 $m^2\ g^{-1}$ for the alkaline-treated material, while the micropore volume was only slightly decreased (from 0.136 to 0.130 ml g^{-1}). Besides substantial mesoporosity development, the zeolite maintained Brønsted acidic properties, which are highly attractive in order to promote acid-catalyzed reactions like glycerol dehydration. Catalytic testing of the modified solids showed an improved performance in dehydration of glycerol to acrolein, due to the unique interplay between improved physical transport in the shortened micropores and the preserved high density of acid sites. The catalyst stability was improved upon desilication due to an increase in coke tolerance. A treatment of both solids in air at 773 K led to a partial regeneration of acid sites for glycerol dehydration.

1. Introduction

Biodiesel production is an attractive alternative to substitute non-renewable fuels, and it is a method for energy production actually in use. The rising worldwide biodiesel production, particularly in Argentina, led to an increasing generation of glycerol and a decrease in its price in the market. Therefore, this situation stimulated the search for alternatives to generate high value-added chemicals [1]. Among the different possibilities, one of the attractive alternatives is the glycerol dehydration to produce acrolein. It is a chemical intermediate for the production of acrylic acid, acrylic acid esters, superabsorbers, polymers and detergents [2]. At present, no acrolein is produced commercially in Argentina, and its production worldwide is done from the selective oxidation of propylene over BiMoOx based mixed oxides [3]. To carry out the reaction of interest it is possible to follow two different paths, liquid-phase or gas-phase reaction. In the first case, there are different operational problems. The harsh conditions together with the presence of liquid acids generate an extremely corrosive medium, resulting in high equipment investments and maintenance costs. As a result, it is unfeasible to produce acrolein commercially from glycerol in liquid phase due to technical and environmental problems, such as reactor corrosion, catalyst/reaction mixture separation and waste management [3]. Besides, in order to avoid excessive loss of selectivity, the conversion has to be limited to 15–25%.

In light of the above-mentioned drawbacks, the scientific community has turned preferentially to the study of the gas phase reaction over solid acid catalysts, such as metal phosphates [4,5], metal sulfates [6,7], metal oxides [8,9], heteropolyacids (HPAs) supported on metal oxides [10,11] and zeolites [12,13]. Furthermore, in many reactions, the traditional liquid-acid catalysts were progressively substituted with zeolite-based processes [14]. Application of these solid-acid catalysts offers several key advantages. Zeolites are environmentally harmless, noncorrosive, and separate easily from the reaction mixture as compared to homogeneous catalysts. In particular, zeolites are used in many catalytic processes because they exhibit good thermal stability, good resistance to the presence of water, large surface area and in this case, a right acid sites density for the desired reaction. Moreover, the shape-selective properties of zeolites related to the presence of an ordered microporous network, can restrict the formation of undesired products by control

* Corresponding author at: Santiago del Estero 2654, (3000) Santa Fe, Argentina. Tel.: +54 342 4533858; fax: +54 342 4531068.
E-mail address: querini@fiq.unl.edu.ar (C.A. Querini).

http://dx.doi.org/10.1016/j.micromeso.2014.11.014
1387-1811/

of reactant or product diffusion as well as the volume available for transition states. But the purely microporous nature of zeolites frequently posses transport limitations, particularly when bulky molecules are involved, which adversely affect catalytic performance. A breakthrough was the synthesis of mesostructured aluminosilicates [15]. Emerging mesoporous materials however generally do not comply with most practical requirements as a result of limited thermal stability and poor acidic properties. Consequently, new synthesis procedures for preparation of small zeolitic crystals [16] or post-treatment procedures to create extra-porosity were increasingly investigated [17–19].

Conventional steaming and acid leaching methods, as well as treatments in alkaline media have been applied to modify several zeolites properties. The latter method removes preferentially Si from the zeolite framework (desilication) [20–22], while the former ones lead to dealumination. Desilication was firstly applied to study chemical changes of MFI crystals upon contact with NaOH solutions, and this treatment has shown to induce a significant mesoporosity in MFI-type zeolites [23–25]. Furthermore, this treatment made it possible in several cases to maintain the crystal structure and the acidic properties of the solids. Besides, mercury intrusion porosimetry measurements on several alkaline-treated zeolites provide convincing evidence that the mesoporosity created upon desilication is fully accessible from the external surface of the zeolite crystals, being crucial when improved molecular transport in the pore system is aimed at [26]. Then, the combined micro- and mesoporous zeolites fabricated by desilication still exhibit shape selective properties, with a shorter micropore diffusion path length and an enhanced access to the micropores via the newly created mesopores.

It was also reported that the mesoporosity and pore size distribution [27] is independent of the crystal morphology, and the mechanism to generate intracrystalline mesoporous is mainly influenced by the Si/Al ratio. Ogura et al. [24] have studied the desilication of H-ZSM5 with a Si/Al ratio equal to 19.7 (NaOH 0.2 M; 353 K; 5 h), and the mesoporous generation was corroborated. Suzuki et al. [23] have analyzed the effects of the alkaline treatment with NaOH 0.5 M on H-ZSM5 Si/Al: 37 varying the duration of the treatment and the temperature of the alkaline solution. It was concluded that the maximum generation of mesopores was obtained at 30 min after treatment initiation and that longer times did not significantly modified the results. Also, a treatment at 323 K was not effective, and a temperature of 343 K was required to achieve adequate mesoporosity and the preservation of the crystal phase. Later, Groen et al. [28] studied the optimum treatment for several zeolites (MFI, BEA, MOR and FERR). They observed that the better conditions (temperature, concentration and time of treatment) depend on their structure, the size of their interconnected channels and the uni-, bi- or tri-dimensional configuration. The optimum treatment on H-ZSM5 (Si/Al: 37) was obtained with 30 ml of NaOH 0.2 M per g of zeolite (OH^-/Si molar ratio equal to 0.4), at 338 K for 30 min [19]. Besides, the strong acid sites concentration increased due to the decreased in the Si/Al ratio, while the acid strength hardly changes. Moreover, the same authors stated that the optimal Si/Al ratio of H-ZSM5 zeolite was in the range of 25–50 [29]. Additionally, a recent study of H-ZSM5 (Si/Al: 47) [30] established that the presence of mesopores does not contribute significantly to increase the amount of Brønsted acid sites, and only influences the accessibility of micropores (shortens the diffusive path).

Desilicated H-ZSM5 zeolites have been investigated in several reactions, including cumene cracking [31], degradation of low-density polyethylene [32], methane dehydroaromatization [33], catalytic cracking of *n*-octane [34], hydroxylation of benzene to phenol [35], methanol to gasoline [36], *n*-hexane isomerization and cracking [37,38], conversion of propanal to gasoline-range molecules [39], the selective production of olefins from bioethanol [40], light olefin production by heavy oil cracking [41] and the eterificación of 1,2-propylene glycol with 1-octene [42]. In most cases, improved activity, stability, and selectivity have been reported. In general, the observed improvement has been ascribed to enhanced diffusion due to the generation of mesopores channels. The versatility of this alkaline treatment opens new avenues to improve diffusion characteristics in zeolite-catalyzed applications.

Regarding the catalytic glycerol dehydration, it has been studied by mean of the utilization of several zeolites (H-ZSM5, H-Beta, H-Y, H-ZSM11) [43] and the obtained results were related with their channel structure. It was determined that H-ZSM5 zeolite performance was better than the obtained by H-Beta and H-Y zeolites. It was demonstrated that H-zeolites with smaller channels, the ones marginally larger than the molecular diameter of glycerol, were preferential for the reaction. It was found that as the channel diameter increased, the selectivity to acrolein was affected. Moreover, H-ZSM11 zeolite with lower channel complexity was more likely to obtain superior catalytic performance due to enhanced diffusion. The results imply that steric hindrance or channel pattern has a stronger influence than acid sites density on coke formation. Regarding acidity, it is accepted that the production of acrolein is catalyzed by Brønsted acid sites, while the Lewis acid sites increase the selectivity to hydroxyacetone [44,45].

To investigate the deactivation by coke deposition during the glycerol dehydration, and to obtain catalysts with higher long-term stability, Possato et al. [46] studied this reaction with different H-ZSM5 zeolites (Si/Al: 15, 25 and 40). Besides, the more siliceous zeolite was treated with NaOH aqueous solutions. Alkaline treatment allowed a rapid diffusion and consequently improved the reaction kinetics. However, the severity of the treatment negatively interfered on the Brønsted and Lewis acid sites relative concentration and, consequently, in the efficiency of the catalysis performed by these materials. On the other hand, during the catalytic reaction the intracrystalline mesopores allowed carbonaceous compounds to be deposited herein, resulting in less blocked micropores. The glycerol conversion and the stability obtained with the alkaline treated zeolite were better than the parent zeolite. However, the catalysts used in their study did not present the best selectivity to acrolein when compared to other catalysts.

To improve the acrolein selectivity, preserving the good conversion and stability, in this paper the glycerol to acrolein dehydration using H-ZSM5 zeolite (Si/Al: 15) modified by alkaline treatment was studied. Although this Si/Al ratio is outside the range recommended by Groen et al. [29], it was reported that the treatment of the less siliceous zeolites allows the formation of narrower mesopores and a less broad pore size distribution. It is expected that as result of the higher Al concentration and due to the modified mesopores size distribution, the acrolein selectivity could improve. On the other hand, water can strongly adsorb on the surface acid sites of the solid acid catalysts and disturb the adsorption of accessible reactants, then, a 20 wt.% glycerol in water solution was fed, which is a more concentrated solution than that used by Possato et al. [46]. Finally, since the selectivity to acrolein obtained with non-treated H-ZSM5 zeolites reported by Gu et al. [43] was successful at a weight hourly space velocity (WHSV) of 1.56 g Gly/(g zeolite·h), in the present work it was investigated the reaction at two different space velocities closed to this WHSV value (0.72 and 3 g Gly/(g zeolite·h)).

2. Experimental

2.1. Catalyst preparation

The commercial zeolite used in this study was an H-ZSM5 provided by Zeolyst (CBV-3020E), with a nominal Si/Al ratio of 15, in the protonic form. For alkaline treatment, ca. 2 g of calcined zeolite

was vigorously stirred in 60 ml of a NaOH solution (0.2 M) at 338 K for 0.5 h, following the procedure previously established for ZSM5 zeolites [47]. The zeolite suspension was then cooled down immediately using an ice bath. The remaining product was filtered, carefully washed until neutral pH, and finally dried at 373 K overnight. This material was named 'alkaline-treated zeolite'. The alkaline-treated samples were converted into the H-form by two consecutive exchanges in 0.5 M NH_4NO_3 aqueous solution, for 2.5 h in reflux followed by air-calcination at 823 K for 2 h. This catalyst was named 'treated zeolite'. The as-received materials were calcined under identical conditions prior to the characterization and hereafter denoted as non-treated.

2.2. Catalyst characterization

2.2.1. N_2 Adsorption–desorption isotherms

Nitrogen adsorption–desorption isotherms were recorded at liquid-nitrogen temperature and relative pressure (P/P_0) interval between 6×10^{-7} and 0.998 on a Quantachrome equipment, which was used to assess the created mesoporosity. Samples were evacuated prior to measurements at 523 K for 3 h under a vacuum of 1×10^{-5} Pa. The BET model [48] was used in the relative pressure range 0.01–0.10 to calculate the total surface area, while the micropore volume and mesopore surface area were derived from the *t*-plot, according to Lippens and de Boer [49]. The pore-size distribution was calculated according to the BJH model [50], applied to the adsorption branch of the isotherm. Although adsorption studies with model materials like MCM-41 and SBA-15 have proven that the BJH pore-size model can lead to an underestimation of the actual mesopore-size up to 40% [51], the model is appropriate for comparing mesopore-size distributions in materials of similar nature.

2.2.2. Microscopy analysis

Scanning electron microscopy (SEM) of the non-treated and treated samples at 25 kV were carried out using an electron microscope (JEOL JSM 35C). In order to ensure that the data collected was representative of the whole sample, scans were made at more than one location. The reproducibility verified indicates homogeneous zeolite particles.

2.2.3. X-ray diffraction and ICP-OES studies

X-ray diffraction patterns were measured in a Shimadzu XD-D1 instrument with a monochromator, CuK_α radiation and a scanning rate of 1 min^{-1}. Si and Al concentrations in the solid materials and in the filtrate obtained upon alkaline treatment were determined by inductively coupled plasma atomic emission spectroscopy (ICP-OES). Measurements were performed in a Perkin Elmer Optima 2100 DV. Samples were dissolved using a mixture of perchloric and nitric acids.

2.2.4. Temperature programmed desorption of pyridine (Py-TPD)

Pyridine TPD experiments were carried out to evaluate the acidity of the samples. The catalysts were pretreated in situ in N_2 flow at 573 K during 1 h. After cooling down to room temperature, three consecutive saturation steps with pure pyridine were performed. After this, pure nitrogen was flowed and the temperature was increased up to 423 K, until no pyridine was detected. The TPD experiments were carried out heating at 12 K min^{-1} in the temperature range 423–1073 K, and pyridine was detected using a FID detector after methanation, using a setup similar to that described in Section 2.3.

2.2.5. FTIR studies

The acidic properties of the samples were also studied by pyridine adsorption followed by infrared spectroscopy (FTIR). Spectral measurements of pyridine adsorption on the samples were performed on a JASCO FT-IR 5300 spectrometer equipped with a DTGS detector. The range and resolution of acquisition were 4600–400 and 4 cm^{-1} respectively. A self-supporting wafer for each sample (~20 mg and 13 mm of diameter) was prepared, placed in a thermostatized cell with CaF_2 windows connected to a vacuum line, and evacuated for 8 h at 673 K. The background spectrum was recorded after cooling the sample to room temperature. Afterward, the solid wafer was exposed to pyridine vapors (Sintorgan, 99% purity) until the system was saturated to 46 mm Hg at room temperature; the contact time at this pressure was 12 h. The IR spectrum for each sample was obtained after pyridine desorption by evacuation for 1 h at 373, 473, 573 and 673 K. All the spectra were recorded at room temperature before and after pyridine adsorption and desorption at each temperature. The difference spectrum was finally obtained by subtracting the background spectrum previously recorded. The integrated molar extinction coefficients values used for quantification were 1.67 cm/μmol for the 1545 cm^{-1} band characteristic of pyridine on a Brønsted acid site and 2.22 cm/μmol for the 1455 cm^{-1} band of pyridine on a Lewis acid site following the procedure of Emeis [52].

2.3. Coke characterization

The coke was characterized by temperature-programmed oxidation (TPO). The experiments were carried out using a modified technique [53] in which the gases coming out of the analysis cell passed through a methanation reactor. A H_2 stream was fed to this reactor, which was loaded with a Ni catalyst, and where CO and CO_2 were converted to CH_4. This compound was continuously measured using a FID detector. Under these conditions (673 K, 6% O_2, 40 ml min^{-1}), a 100% conversion of CO_x was reached and in this way the sensitivity of the technique was greatly improved. The analysis cell was loaded with approximately 10 mg of used catalyst and the analyses were performed employing a heating rate of 12 K min^{-1} starting from 293 K. Equipment calibrations were performed using pulses of CO_2 diluted in He.

2.4. Catalytic activity

The dehydration of glycerol was conducted at atmospheric pressure in a continuous fixed-bed stainless steel reactor, using 0.4 g of catalyst (particle size 40–80 mesh) without diluents. Prior to the catalytic tests, catalysts were pretreated at 573 K in N_2 flow for 1 h to remove adsorbed water. The reaction feed was an aqueous solution containing glycerol (20 wt.%). It was evaporated in a preheater at 533 K, with 50 ml min^{-1} of N_2 as carrier gas, and was introduced in the system at different rates to evaluate the effect of space velocity. It is well known that diffusion is driven by the concentration difference between internal and external space of catalyst [54]. The introduction of carrier gas could enlarge the concentration difference by supplying glycerol (and removing products) continuously to (and from) outer space of catalyst, which could stimulate the diffusion of glycerol into channels and products out of channels of H-zeolites, resulting in higher glycerol conversion and acrolein selectivities. Throughout this work, the space velocity used (WHSV) represents the mass of glycerol per gram of catalyst, per hour. The reactor was placed in an electrically heated furnace. After the reaction, the carrier flow was maintained for 1 h, in order to purge the system.

Reaction products together with the unconverted glycerol were collected in a cold trap maintained at 278 K at 30 min intervals. The analysis of the products was carried out offline in a Shimadzu gas chromatograph (GC) equipped with a Phenomenex ZB-5 capillary column (30 m × 0.25 mm × 0.25 μm) and a flame ionization detector (FID). The following products have been identified and

quantified: acrolein, acetaldehyde, propanal, and acetol. Other compounds in low concentrations have not been identified. A volumetric method was employed to determine the quantity of glycerol in the collected samples [55]. The following equations were used to calculate glycerol conversion, product yield and selectivity:

$$\text{Glycerol conversion}(\%) = \frac{n_{gly}input - n_{gly}output}{n_{gly}input} \times 100$$

$$\text{Product yield } (\%) = \frac{n_j output}{v.n_{gly}input} \times 100$$

$$\text{Product selectivity } (\%) = \frac{\text{product yield}}{\text{glycerol conversion}} \times 100$$

where $n_{gly}input$ and $n_{gly}output$ are the molar flow of glycerol at the input and output of the reactor; n_j is molar flow of the product j, and the coefficient v represents the ratio between the number of carbon atoms in a molecule of glycerol and the number of carbon atoms in a molecule of product obtained, being 1.5 for acetaldehyde and 1 for the other products observed in this study, all of them containing three carbon atoms.

3. Results and discussion

3.1. Catalysts characterization

3.1.1. Surface area and pore volume

The conditions used in this work to treat the zeolite had the objective of obtaining a substantial increase in the mesoporosity while preserving the intrinsic properties of the zeolite, such as a high surface area, shape selectivity, and acidity. These conditions were selected by Groen et al. [19,28], based on an exploratory program with a broad range of alkaline treatment conditions (time, temperature, and alkaline concentration), to assess appropriate conditions for mesoporosity development in various zeolite structures. Fig. 1A shows the N_2 adsorption and desorption isotherms at 77 K for the non-treated (a) and treated zeolites (b). The non-treated materials generally exhibit a type I isotherm with a plateau at high relative pressures, as a result of the microporous nature of the material with limited mesoporosity. Besides, a type H4 hysteresis was observed, and since this zeolite displayed a type I isotherm, this hysteresis is also a sign of microporosity [56,57]. Upon alkaline treatment in NaOH and subsequent ion exchange the treated zeolitic structure showed an enhanced uptake of N_2 at higher relative pressures accompanied by a hysteresis loop, being indicative of extra mesoporosity [18]. The BJH [50] pore size distribution derived from the adsorption branch of the isotherm confirmed the increased mesoporosity in the treated zeolites (Fig. 1B), and shows in particular a slightly broad distribution of mesopores.

The mesopore diameter estimated from pore size distribution derived from N_2 adsorption was 60 Å. The BET [48] surface areas derived from the isotherms in Fig. 1A are listed in Table 1, and evidence that the treated zeolites can be used more effectively in terms of porosity than the non-treated zeolite, in view of the generally higher surface areas of the former. Although the validity of the BET model for surface area calculations on microporous materials is questionable [58], the surface areas derived from this model in the adopted pressure range P/P_0 = 0.01–0.10 can still be used for comparative purposes. Application of the *t*-plot [59] indicated that a significantly increased mesoporosity (325 $m^2\ g^{-1}$) was developed in the treated zeolites compared to the non-treated zeolites. It is important to emphasize that the microporous structure was not significantly affected by the treatment; only a slight decrease in microporosity (4.5%) was observed. This result is consistent with those found in the literature [60].

3.1.2. XRD and SEM analyses

XRD patterns presented in Fig. 2A show that the MFI structure was maintained in the treated sample. However, the alkaline treatment did influence the degree of crystallinity in this sample. The variation in crystallinity of the desilicated zeolite resulted to be 10%, and was calculated based on the relative intensities of the reflection peak at 23° (2θ), taking the crystallinity of the parent sample to be 100%. The crystallinity reported by others researchers indicate similar values [57]. Therefore, X-ray diffraction analysis confirmed the preservation of the long-range crystal ordering in the samples, with a decrease in the intensity of the characteristic reflections. The SEM micrographs of the samples are shown in Fig. 2B and C. SEM analysis showed that the zeolite particles size is in the range of 0.5–3 μm. All samples consist of similar particles associated with smaller crystallites and larger agglomerated crystals, as other researchers previously observed [31,36]. The alkali treatment results in no visually-detectable changes in the general morphology of the particles. The particles of the alkaline-treated sample have a slightly rougher surface, and this is in accordance with the adsorption isotherms.

3.1.3. Elemental composition and pyridine TPD analyses

ICP-OES measurements in both the filtrate and the solid material confirmed the preferential leaching of Si, leading to a lower Si/Al ratio in the treated materials (Table 1). The fact that Al is more difficult to extract can be explained by the negative charge associated with Al tetrahedra in the zeolite framework, due to the trivalent oxidation state of aluminum. This hinders the

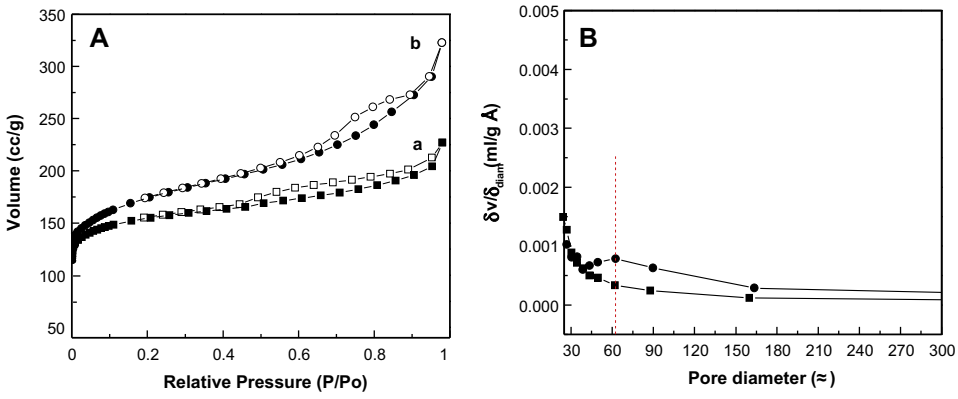

Fig. 1. (A) N_2 adsorption–desorption isotherms: (a) non-treated H-ZSM5; (b) treated H-ZSM5. (■; ●) Adsorption; (□; ○) desorption. (B) BJH pore size distribution: (■) non-treated H-ZSM5; (●) treated H-ZSM5.

Table 1
Catalysts physical properties and elemental composition.

Catalysts	BET area (m^2/g)	Mesop. area (m^2/g)	Microp. vol. (cc/g)	Si/Al (mol/mol)
H-ZSM5 non-treated	579	254	0.136	15.2
H-ZSM5 treated	627	325	0.130	13.9

extraction of Al through hydrolysis of Si—O—Al bonds, by negatively charged hydroxyl groups [61] compared to the relatively easy cleavage of the Si—O—Si bond in the absence of neighboring Al tetrahedra [21].

The number of strong acid sites in the treated zeolites is generally increased due the lower Si/Al ratio, while the acid strength hardly changes. It was reported that the desilication treatment hardly affects the acidic properties of various zeolites. Moreover, an increased ammonia uptake over alkaline treated H-ZSM5 zeolites has been determined by NH_3-TPD experiences [29]. The enhanced acidity was clearly assigned to the higher Al content relative to Si, in the alkaline-treated zeolites giving rise to a higher density of acid sites.

The effects of desilication on the acidity of the H-ZSM5 zeolites were studied by TPD of adsorbed pyridine, as shown in Fig. 3. It has been generally accepted that the TPD peak position is directly related to the strength of the acid sites. Therefore, the low-temperature desorption peaks are due to the weak acid sites, while the high-temperature desorption peaks are due to the strong acid sites. For the non-treated sample, two distinct desorption peaks were observed at 525 and 925 K in the Py-TPD profile. By mean of NH_3-temperature programmed desorption experiences over H-ZSM5 zeolites, some researchers [12,62] assigned the high and low temperature peaks to Brønsted and Lewis acid sites, respectively. Here, Py-desorption peaks between 433 and 673 K are related to weak acid sites while peaks at temperatures higher than 873 K are assigned to strong acid sites. The non-treated zeolite desorption profile showed a peak at high temperature. After alkaline treatment, the acid site distribution on the alkaline treated zeolite changes drastically due to exchange of zeolitic protons by sodium cations, generating Lewis acid sites. This affirmation is supported by Esquivel et al. [63], who observed on β-zeolite ion exchanged with Na(I), a decrease in the number of medium and strong acid sites while the population of weak acid sites increased. These observations revealed that medium–strong Brønsted acid sites were those preferably exchanged by the cations, thus decreasing their populations. Also, it was suggested [63] that the exchanged cations act as acid sites of Lewis nature able to coordinate several pyridine molecules

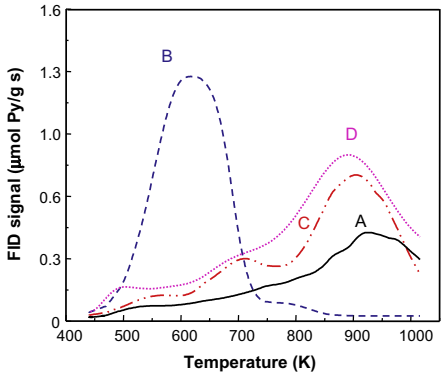

Fig. 3. Pyridine TPD profiles for fresh catalysts: (A) non-treated H-ZSM5; (B) H-ZSM5–alkaline treatment; (C) H-ZSM5–alkaline treatment (1 I.E.); and (D) H-ZSM5–alkaline treatment (2 I.E.).

Table 2
Acidic properties of the fresh catalysts.

Catalysts	Acidity (mmol g^{-1})
H-ZSM5 non-treated	0.592
H-ZSM5 alkaline treatment	1.131
H-ZSM5 alkaline treatment (1 I.E.)	1.014
H-ZSM5 alkaline treatment (2 I.E.)	1.238

which are desorbed at lower temperatures, and consequently the population of the weak acid sites was raised. Similar observations were carried out with Na-modified H-ZSM5 catalysts [64].

After two successive ion exchanges with ammonium nitrate, there was a recovery of the strong acid sites and an increase of the amount thereof, as a result of the increasing number of aluminum network sites exposed after the alkali treatment, as also indicated by the decrease in the Si/Al ratio upon this treatment. The quantity of pyridine desorbed is summarized in Table 2. Acid sites available for reaction increased from 0.592 to 1.238 mmol g^{-1}. The high acidity of the solid subjected to alkaline treatment (H-ZSM5-Alkaline treatment) is mainly due to weak Lewis sites. After the alkaline treatment, and ion exchange with ammonium, it can be observed in Fig. 3 (compare curve A with curves C and D) that the peak ascribed to strong acid sites gradually shifts to lower temperatures. These changes are accompanied by a gradual increase in the intensity at intermediate temperatures (673–773 K). These changes either indicate that desilication converts some of the strong Brønsted acid sites into sites of weaker acidity, or modifies

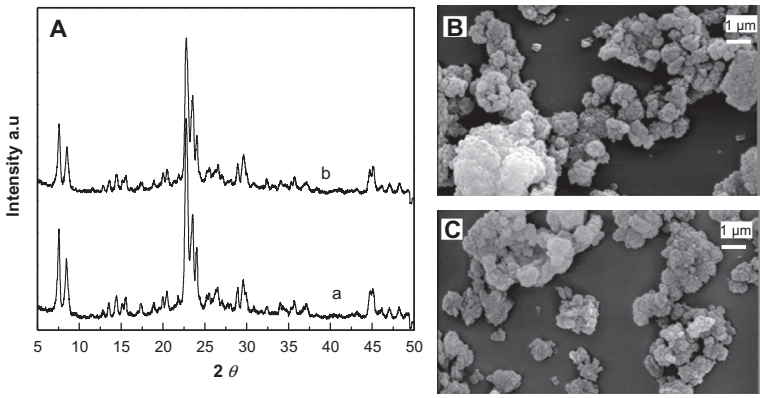

Fig. 2. (A) XRD spectra for fresh catalysts: (a) non-treated H-ZSM5; (b) treated H-ZSM5; (B and C), SEM micrographs of the treated and non-treated samples, respectively.

the accessibility of these sites due to the partial removal of silica. This affirmation was reported by other authors [39].

3.1.4. FTIR studies

As a result of preferential silicon extraction, the Si/Al ratio in the treated zeolite is lower than in the non-treated sample and thus the number of potential Brønsted acid sites per unit weight should be increased. ^{27}Al and ^{29}Si MAS-NMR patterns recorded for non-treated and alkaline-treated ZSM5 zeolites have shown to be very similar, with a negligible contribution from non-framework aluminum species [47]. This suggested that the aluminum was predominantly tetrahedrally coordinated in the zeolite framework upon alkaline treatment. In agreement, FTIR and NH_3-TPD investigations have revealed a preservation of the acidity. The IR absorption band typical for Brønsted acidity at 3610 cm^{-1} remained present and the acid strength in the treated zeolites derived from NH_3-TPD was similar to that in the non-treated samples. Moreover, the total acidity indeed increases correlating with the higher aluminum content relative to the silicon in the alkaline-treated zeolite [47].

Infrared measurements of adsorbed pyridine were performed. The region of the FTIR spectrum that corresponds to the hydroxyl groups are shown in Fig. 4A and B, for the non-treated and treated H-ZSM5 catalysts, respectively. Five zones can be distinguished in the spectral range of hydroxyl stretching modes. The most intense bands are displayed in the range 3725–3750 and 3610–3615 cm^{-1} approximately, and at around 3664, 3680 and 3781 cm^{-1}.

On the non-treated catalyst (Fig. 4A) the shoulder observed in the signal at 3744 cm^{-1} represents isolated Si—OH groups not interacting significantly with other species. These sites are commonly claimed to be located on the external surface of the zeolite, as they are perturbed upon adsorption of steric-demanding probe molecules not able to access the micropore system of the zeolite. The intensity of this peak (3744 cm^{-1}) has previously been correlated with the external surface area and thus the average crystal size of the zeolite [65–67]. Bands with maxima at 3730 and 3680 cm^{-1} are clearly visible. These bands have been associated with nearly free Si—OH sites predominantly located inside the structure as they remain virtually unperturbed upon adsorption of large molecules [36]. As expected, the band representing the bridging strongly acidic Al(OH)Si sites, is located at around 3615 cm^{-1}. Finally, several bands at lower frequencies are assigned to a variety of internally located Si—OH sites involved in relatively strong hydrogen bonds. The location assignments (internal or external) of the various sites have been confirmed in a more extensive spectroscopic study using large probe molecules (2,4,6-trimethyl pyridine) [68]. An H-ZSM5 free from internal defects will only have a Si—OH contribution from the external surface (giving a peak at 3744 cm^{-1}). Thus, the remaining Si—OH components located at lower frequencies for the non-treated H-ZSM5 sample represent internal defects in the framework.

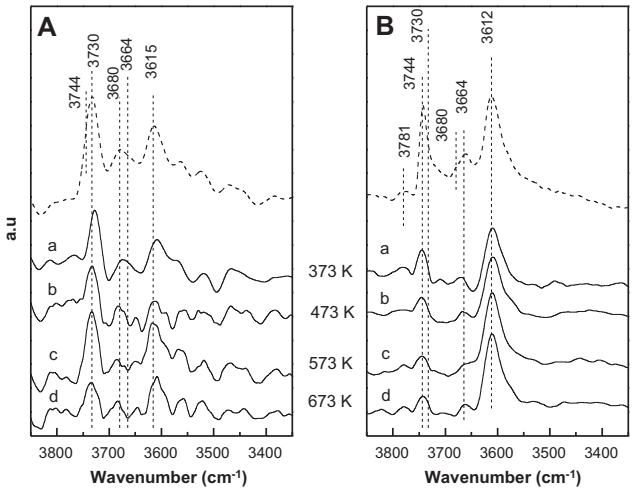

Fig. 4. FTIR spectra in the hydroxyl region for the catalysts: (A) non-treated H-ZSM5; (B) treated H-ZSM5. Fresh catalysts: dashed lines. Difference between the spectra recorded before and after pyridine adsorption–desorption: continuous lines. Pyridine desorption at: (a) 373 K; (b) 473 K; (c) 573 K and (d) 673 K.

Upon NaOH treatment and subsequent ion exchange, the vibrational properties of the sample in the σ(O—H) region changed substantially, as shown in Fig. 4B. The 3744 cm^{-1} band increased in intensity, whereas the different Si—OH contributions at lower frequencies vanished, implying that after the treatment the Si—OH sites are more uniform and to a much larger extent, isolated. The interpretation of this observation is not straightforward, but according to these results, the defects became part of the mesopores which effectively may appear like an ordinary external surface with isolated Si—OH sites represented by the band at 3744 cm^{-1}. In any case, it is beyond any doubt that the features characterizing Si—OH in structural defects are clearly reduced. It should also be mentioned that the NaOH treatment inevitably seems to generate Al—OH species, in which Al atoms belong either to EFAL species (extra framework aluminum species), or to tri-coordinated atoms linked to the framework by two O atoms [69], which give rise to the rather small components at 3664 and 3781 cm^{-1} clearly seen for the treated samples. These signals are not due to the acidic character of the corresponding OH groups, but to the Lewis acidity of the Al atoms to which they are linked [69–71]. Based on FTIR and quantum chemical modeling, Brand et al. [70] suggested that the band at 3666 cm^{-1} (close to our observed band at 3664 cm^{-1}) can be assigned to terminal and bridging OH groups in dimeric $(Al(OH)_3)_2$ species. Also Fleischer et al. [71] found that the ^{1}H NMR chemical shift of the bridging protons in the $(Al(OH)_3)_2$ species is in the range assigned to OH groups associated with extra framework Al species.

To identify the nature of the acid groups, the effect of pyridine adsorption on the intensity of the various OH bands was determined on the two samples. Fig. 4 shows the spectra obtained as the difference between the spectra recorded before and after pyridine adsorption–desorption at 373, 473, 573 and 673 K (solid lines). These spectra represent the acid groups which are occupied by adsorbed pyridine in both samples at each desorption temperature. The spectra obtained in this way for the non-treated samples shown in Fig. 4A (continuous lines), show intense signals at 3730 and 3615 cm^{-1}. The intensity of the signal at 3730 cm^{-1} (free Si—OH sites predominantly located inside the structure) did not decreased for desorption temperatures up to 573 K, indicating that these are strong acid sites. The signals at 3615 and 3680 cm^{-1} have a similar behavior, while the signal at 3664 cm^{-1} vanish at 473 K, therefore the sites associated with this latter signal have low acidity. Regarding to the treated sample, the intensity of the band at 3612 cm^{-1} (bridging strongly acidic Al(OH)Si sites) observed in the spectra after pyridine desorption at 373, 473, 573 and 673 K, is comparable to the original signal, what indicates that almost all these sites have strong acidity, because its intensity was not modified when the desorption temperature was increased. On the other hand, the signal at 3744 cm^{-1} decreased when desorption temperature was increased, and then, these acid species (external Si—OH) have lower acid strength. It is interesting to highlight that all the groups represented by these signals, interacted with pyridine and therefore represented acid sites available for the reaction.

In summary, the main difference between the treated and non-treated catalysts is the concentration and accessibility of acid silanols that corresponds to the FTIR spectrum in the 3700–3750 cm^{-1}, and the concentration and acid strength of bridging

hydroxyl groups (around 3615 cm^{-1}). These results indicate that the preparation procedure followed to obtain the treated H-ZSM5 catalyst increased both the concentration of bridging hydroxyl groups (around 3615 cm^{-1}) and the external Si—OH (3744 cm^{-1}), and this fact may be the reason of the superior catalytic performance of this catalyst, as will be shown below.

The signals associated to chemically adsorbed pyridine are displayed in the range 1700–1400 cm^{-1}, and shown in Fig. 5. Pyridine adsorbed on H-ZSM5 catalysts resulted in the appearance of bands characteristic of pyridine adsorbed on the Lewis acid sites (PyL) at 1622 and 1450 cm^{-1}, on Brønsted acid sites at approximately 1544 and 1636 cm^{-1} (PyH^+), and the bands attributed to pyridine adsorbed on both Brønsted and Lewis acid sites at 1490 cm^{-1} [72,73]. Fig. 5B shows that as a result of the alkaline treatment followed by two ion-exchange steps with NH_4NO_3 solution, an increase in the total intensity of the signals was observed on the treated zeolite. There is an important increase in the relative size of the signal at 1544 cm^{-1} indicating that the concentration of framework Al sites on the surface of the treated sample increased. This is because the greater BET area and mesoporosity obtained upon the alkaline treatment led to a higher exchange of NH_4^+ that were transformed in H^+ by calcination. Because of this, the intensity of the bands attributed to pyridine bonded to Brønsted acid sites increased.

The concentrations of Brønsted and Lewis acid sites were estimated from the intensities of the band at 1544 and 1450 cm^{-1} respectively, following the procedure of Emeis [52]. These values were used to calculate the relation between the Brønsted (B) and the Lewis (L) sites for all the samples. The acid sites concentration determined in this way upon pyridine desorption at several temperatures are detailed on Table 3. For example, at 473 K it was 259 μmol g^{-1} for non-treated H-ZSM5 catalyst (210 and 49 μmol g^{-1} for Brønsted and Lewis sites, respectively), and 382 μmol g^{-1} for treated zeolite (327 and 55 μmol g^{-1} for Brønsted and Lewis sites, respectively). These results showed a higher concentration of Brønsted acid sites accessible to pyridine on the treated sample. These Brønsted sites are proposed as the catalytic species where the dehydration of glycerol to acrolein is performed [44,45]. The B/L ratios obtained with these analyses are also included in Table 3.

Information on the strength of Lewis and Brønsted acid sites was obtained from pyridine thermodesorption, taking spectra at different desorption temperatures and quantifying the acid sites

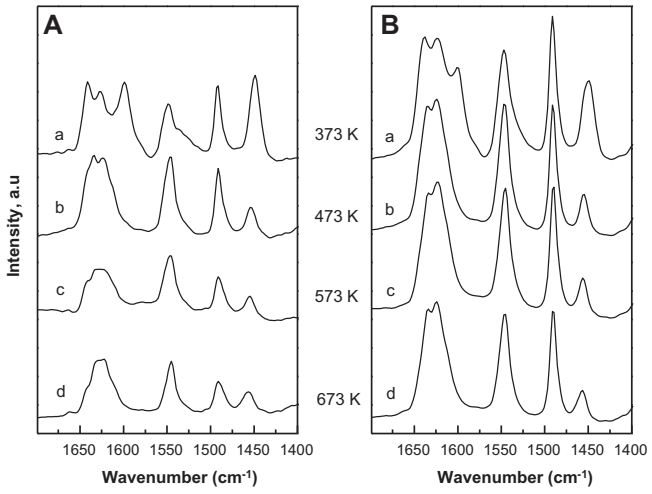

Fig. 5. FTIR spectra in the pyridine region after adsorption and desorption at (a) 373 K; (b) 473 K; (c) 573 K and (d) 673 K. (A) Non-treated H-ZSM5 and (B) treated H-ZSM5.

Table 3
Acid sites characterization: Lewis and Brønsted sites concentrations determined by FTIR analyses of adsorbed pyridine.

Temperature (K)	μmol g^{-1}			B/L
	B	L	B + L	
Non-treated H-ZSM5				
373	219.8	120.3	340.1	1.83
473	209.8	49.5	259.3	4.24
573	158.3	22.3	180.5	7.11
673	151.8	21.5	173.3	7.07
Treated H-ZSM5				
373	335.7	152.0	487.7	2.21
473	327.1	54.7	381.7	5.98
573	326.5	45.5	371.9	7.18
673	275.0	45.0	320.1	6.11

at each temperature. From the values in Table 3, weak, medium and strong acid sites can be obtained. Subtracting the number of sites obtained at 373 and 473 K the weak acid sites were calculated. Then, if the subtraction is performed between the quantities obtained after desorption at 473 and 573 the concentration of medium strength acid sites was calculated. Finally, the strong acid sites were those that remain at 573 K. Table 4 shows that on the treated sample almost the total amount of Brønsted sites are strong (326 μmol g^{-1}), and the majority of Lewis sites has low acidity (97 μmol g^{-1}). The ratio between both strong Brønsted and Lewis sites on treated zeolite is similar to the value of the non-treated zeolite.

3.2. Catalytic activity

The main products identified by GC analysis were acrolein, acetaldehyde, propanal, and acetol. Besides, some chromatographic signals in lower quantities have not been identified. Fig. 6A and B shows the activity results obtained with the non-treated and the treated catalysts, at a space velocity of WHSV = 3 h^{-1} (g glycerol (g catalyst)$^{-1}$ h^{-1}), at 548 K. Under these conditions, the results of conversion and selectivity to acrolein obtained using the treated zeolite as catalyst, were superior to those obtained on the non-treated zeolite (Fig. 6A and B). The higher conversion of glycerol on the treated catalyst as a function of time on stream (Fig. 6A) suggests that the increased surface area attenuate the catalyst deactivation by coke formation. It has been reported in previous studies that the geometry of channels and the intracrystalline diffusivity have great impact on the formation of coke [43]. Besides, the selectivity to acrolein of both catalysts is about of 80% (Fig. 6B). Using this space velocity, the conversion level is low for both zeolites, as a consequence of the relatively low residence time of the glycerol in the reactor.

Fig. 6C and D shows results obtained at a lower space velocity (WHSV = 0.75 h^{-1}). It can be observed that the selectivity to

Table 4
Acid sites characterization: acid strength distribution.

Acid sites strength	μmol g^{-1}			B/L
	B	L	B + L	
Non-treated H-ZSM5				
Weak	10.1	70.8	80.9	0.14
Medium	51.5	27.2	78.7	1.89
Strong	158.3	22.3	180.5	7.11
Treated H-ZSM5				
Weak	8.6	97.4	106	0.09
Medium	0.6	9.2	9.8	0.07
Strong	326.5	45.5	371.9	7.18

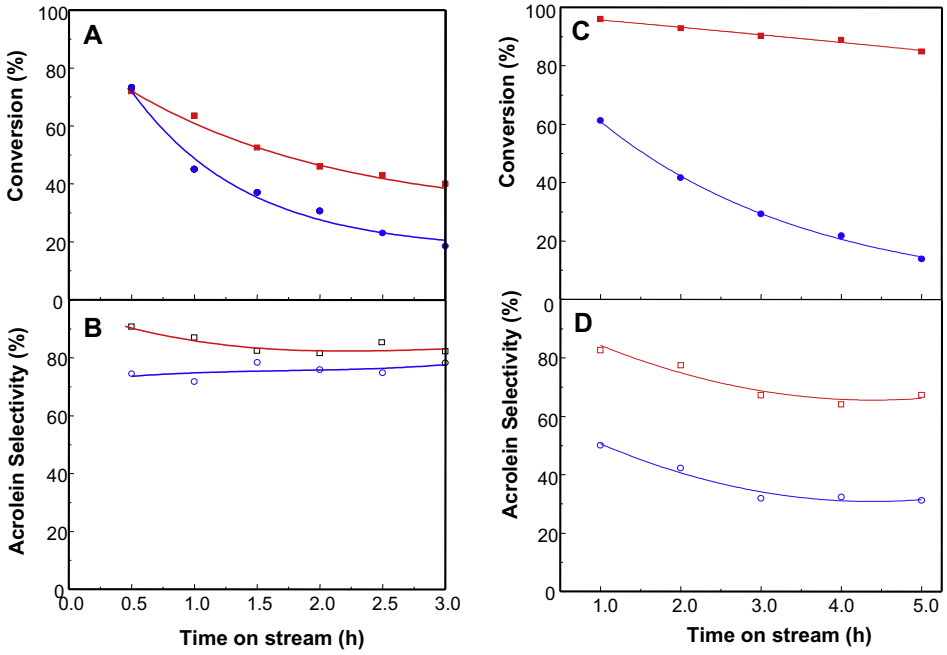

Fig. 6. Glycerol conversion (A) and acrolein selectivity (B) with time on stream; $T = 548$ K; WHSV = 3 h^{-1}. Glycerol conversion (C) and acrolein selectivity (D) with time on stream; $T = 548$ K; WHSV = 0.75 h^{-1}. Non-treated H-ZSM5 (●; ○) and treated H-ZSM5 (■; □).

Table 5
Catalysts conversion, acrolein yield and selectivities.

Catalyst	WHSV: 3 h^{-1}				WHSV: 0.75 h^{-1}			
	Non-treated H-ZSM5		Treated H-ZSM5		Non-treated H-ZSM5		Treated H-ZSM5	
	TOS* 1 h	TOS 3 h	TOS 1 h	TOS 3 h	TOS 1 h	TOS 5 h	TOS 1 h	TOS 5 h
Conversion (%)	45.1	24.3	63.5	31.5	61.2	13.8	89.6	77.6
Acrolein yield (%)	32.3	19.0	55.2	26.1	30.6	4.5	72.1	58.6
Selectivity (%)								
Acetaldehyde	1.1	0.6	1.2	0.8	1.8	1.4	9.6	1.2
Propanal	0.8	0.6	1.6	0.8	1.3	0.4	7.1	1.1
Acrolein	71.8	78.2	86.9	82.9	50.1	32.4	80.4	69.5
Acetol	2.4	1.4	1.3	0.8	8.3	6.2	0	3.7
Others	21.0	19.2	8.8	14.7	38.6	59.6	2.9	24.5

*Time on stream.

acrolein of the non-treated catalyst decreased (Fig. 6D) and the conversion slightly increased (Fig. 6C), as a result of longer contact time. On the other hand, the treated zeolite showed a conversion level significantly higher at this lower space velocity (compare Fig. 6A and C), while the selectivity to acrolein was around 80% and was not significantly affected by the longer residence time in the reactor (Fig. 6D). It is also very important to highlight that the conversion was more stable in the treated zeolite, with a conversion between 85% and 90% during 5 h (Fig. 6C). Therefore, the modification of the morphology and the acidity obtained with the alkaline treatment was important in order to increase the acrolein production. As shown in Table 4, the main difference in acidity between the two catalysts, is the higher concentration of strong acid sites, maintaining the ratio of Brønsted to Lewis acid sites.

Table 5 shows the glycerol conversion and selectivities to different products at 1 h time on stream, and at the end of the catalytic test. The alkaline treatment and subsequent ion exchanges led to and improvement in the conversion and selectivity to acrolein. As catalyst deactivates, the main change in the selectivity occurs in the 'others' non identified compounds, what indicates that these are mainly final products in the reaction network.

3.3. Coke characterization

The formation of carbonaceous deposits during the reaction was quantified by temperature programmed oxidation of the used catalysts (Fig. 7). In the treated zeolite, for both WHSV studied, there was an increase in the amount of coke formed as a result of the increased availability of acid sites. The coke percentage in the starting zeolite at the two space velocities used in this study, i.e. WHSV = 0.75 and 3 h^{-1}, were 12.85% and 13.01%, respectively; while in the modified zeolite the values of coke content were 14.76% and 17.63%. The greatest amount of coke deposited on the modified catalyst is associated with a better utilization of the inner surface, lowering the pore mouth blockage that occurs on micropores faster than on the mesopores, and also due to the higher acid sites density obtained in the treated zeolite as compared to the original material. The higher acid sites density leads also to a faster coke deposition due to oligomerization. As shown in Table 2, the number of acid sites as measured by pyridine TPD, in the treated-zeolite is almost double than in the parent zeolite. Nevertheless, the amount of coke deposited on the former catalyst was only between 15% and 35% higher (data shown in Fig. 7). These

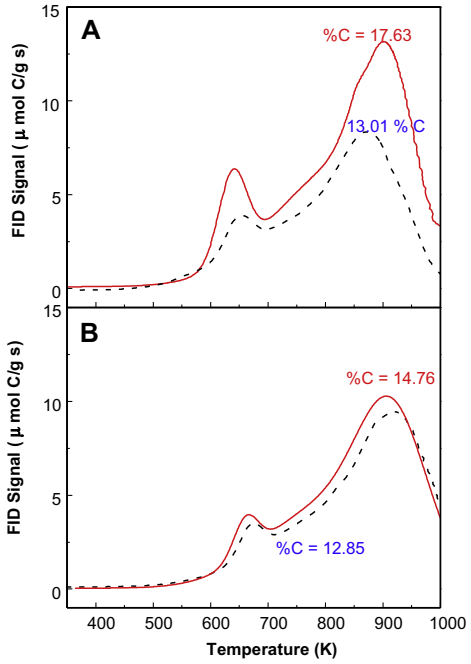

Fig. 7. Temperature programed oxidation profiles of used catalysts. (A) WHSV: 3 h^{-1} (B) WHSV: 0.75 h^{-1}. Non-treated H-ZSM5 (dashed lines) and treated H-ZSM5 (solid lines).

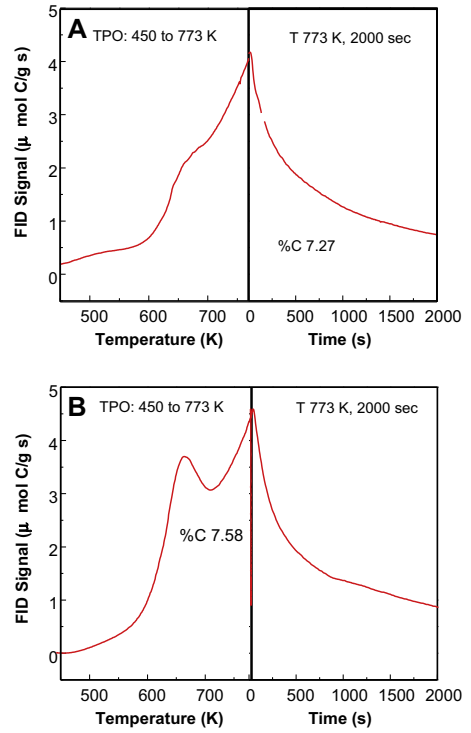

Fig. 8. Regeneration with O_2/N_2 flow of (A) used non-treated catalyst and (B) used treated catalyst. *T*: 773 K, 2000 s.

results also explain the better stability of the treated-zeolite, because the amount of coke per number of acid sites is lower in the treated catalyst.

In order to obtain information regarding the coke removal and acid sites recovery, the catalysts used in glycerol dehydration with a WHSV of 0.75 h^{-1}, were treated in an oxygen/nitrogen mixture at 773 K during 40 min. Fig. 8 shows the TPO profiles obtained in these experiments for both catalysts. The treatment removed

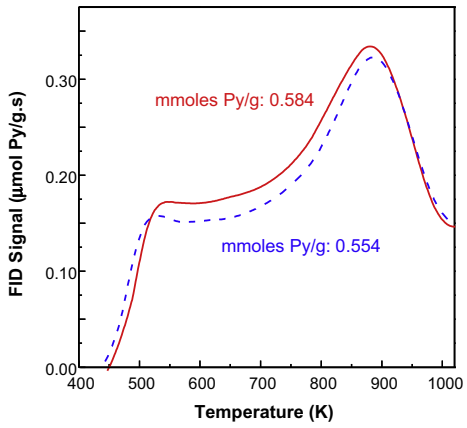

Fig. 9. Pyridine-temperature programed desorption profiles of regenerated catalysts. Non-treated H-ZSM5 (dashed line) and treated H-ZSM5 (solid line).

7.27 and 7.58%C from the non-treated (Fig. 8A) and the treated (Fig. 8B) catalysts respectively, what represents approximately 50% of the initial amount of coke present on the catalysts. The amount of acid sites recovered with this treatment was quantified by pyridine TPD. Fig. 9 shows the results. It was possible to regenerate the acid sites, obtaining 0.554 and 0.584 mmol de Py per gram, for the treated and non-treated zeolites, what represents a significant proportion of the initial available acid sites.

4. Conclusions

In this work, it has been shown that intracrystalline mesopores formation by desilication in alkaline medium resulted in hierarchical porous zeolites. The mesopore size and volume can be controlled using an adequate treatment time and temperature, following the procedure established in previous works [47]. Under these suitable conditions the original zeolitic properties, including acidity, micropore size, and long-range ordering are preserved. Since intracrystalline porosity is developed, desilication of H-ZSM5 zeolites by alkaline treatment opens novel avenues for catalyst design by improved diffusion characteristics, and thus a better utilization of the zeolite crystal for the dehydration of glycerol to acrolein.

N_2-adsorption experiments have shown that optimization of the alkaline treatment of H-ZSM5 zeolite leads to a combined porous material with an increased mesoporosity and preserved microporosity. The mesopores formation is a result of preferential dissolution of Si from the zeolite framework.

The treatment of the zeolite has a pronounced effect on the acidity, increasing mainly the amount of strong Brønsted acid sites, and also decreasing the internal structural defects.

Finally, the improvement in activity and selectivity to acrolein obtained with the treated solid is remarkable, and is due both to the reduction of diffusional limitations as to the increase the number of acid sites accessible to the reaction. The improved stability is assigned to the increased surface area, which causes that the formation of coke has an attenuated inhibitory effect. Preliminary regeneration experiments indicated that a treatment in the presence of oxygen at 773 K recovered a significant proportion of acid sites, by removing approximately half of the initial amount of coke present on the catalysts after the reaction.

Acknowledgments

The authors wish to acknowledge the financial support received from CONICET (PIP 2010-093), UNL (PACT 69) and ANPCyT (PICT 2010-1526).

References

[1] N. Wörz, A. Brandner, P. Claus, J. Phys. Chem. C 114 (2010) 1164–1172.
[2] M. Pagliaro, R. Ciriminna, H. Kimura, M. Rossi, C.D. Pina, Angew. Chem. Int. Ed. 46 (2007) 4434–4440.
[3] Y. Moro-Oka, W. Ueda, Adv. Catal. 40 (1994) 233–273.
[4] F. Wang, J.L. Dubois, W. Ueda, J. Catal. 268 (2009) 260–267.
[5] F. Wang, J.L. Dubois, W. Ueda, Appl. Catal. A Gen. 376 (2010) 25–32.
[6] S.H. Chai, H.P. Wang, Y. Liang, B.Q. Xu, Green Chem. 9 (2007) 1130–1136.
[7] F. Cavani, S. Guidetti, L. Marinelli, M. Piccinini, E. Ghedini, M. Signoretto, Appl. Catal. B Environ. 100 (2010) 197–204.
[8] L.Z. Tao, S.H. Chai, Y. Zuo, W.T. Zheng, Y. Liang, B.Q. Xu, Catal. Today 158 (2010) 310–316.
[9] J. Deleplanque, J.L. Dubois, J.F. Devaux, W. Ueda, Catal. Today 157 (2010) 351–358.
[10] A. Alhanash, E.F. Kozhevnikova, I.V. Kozhevnikov, Appl. Catal. A Gen. 378 (2010) 11–18.
[11] B. Katryniok, S. Paul, M. Capron, C. Lancelot, V. Bellière-Beca, P. Rey, F. Dumeignil, Green Chem. 12 (2010) 1922–1925.
[12] Y.T. Kim, K.D. Jung, E.D. Park, Microporous Mesoporous Mater. 131 (2010) 28–36.
[13] C.J. Jia, Y. Liu, W. Schmidt, A.H. Lu, F. Schüth, J. Catal. 269 (2010) 71–79.
[14] H.F. Rase, Handbook of Commercial Catalysts, CRC Press, Boca Raton, 2000.
[15] C.T. Kresge, M.E. Leonowicz, W.J. Roth, J.C. Vartuli, J.S. Beck, Nature 359 (1992) 710–712.
[16] B. Vogel, C. Schneider, E. Klemm, Catal. Lett. 79 (2002) 107–112.
[17] S. Van Donk, A.H. Janssen, J.H. Bitter, K.P. de Jong, Catal. Rev. 45 (2003) 297–319.
[18] J.C. Groen, L.A.A. Peffer, J. Pérez-Ramírez, Microporous Mesoporous Mater. 60 (2003) 1–17.
[19] J.C. Groen, L.A.A. Peffer, J.A. Moulijn, J. Pérez-Ramírez, Colloids Surf. A (2004) 53–58.
[20] R. Le Van Mao, S.T. Le, D. Ohayon, F. Caillibot, L. Gelebart, G. Denes, Zeolites 19 (1997) 270–278.
[21] A. Cizmek, B. Subotic, I. Smit, A. Tonejc, R. Aiello, F. Crea, A. Nastro, Microporous Mater. 8 (1997) 159–169.
[22] J. Pérez-Ramírez, F. Kapteijn, J.C. Groen, A. Domenech, G. Mul, J.A. Moulijn, J. Catal. 214 (2003) 33–45.
[23] T. Suzuki, T. Okuhara, Microporous Mesoporous Mater. 43 (2001) 83–89.
[24] M. Ogura, S.-H. Shinomiya, J. Tateno, Y. Nara, E. Kikuchi, M. Matsukata, Chem. Lett. (2000) 882–883.
[25] J.C. Groen, J. Pérez-Ramírez, L.A.A. Peffer, Chem. Lett. (2002) 94–95.
[26] J.C. Groen, S. Brouwer, L.A.A. Peffer, J. Pérez-Ramírez, Part. Part. Syst. Charact. 23 (2006) 101–106.
[27] J.C. Groen, L.A.A. Peffer, J.A. Moulijn, J. Pérez-Ramírez, Nanoporous materials IV, in: A. Sayari, M. Jaroniec (Eds.), Studies in Surface Science and Catalysis, vol. 155, Elsevier, Amsterdam, 2005, pp. 401–408.
[28] J.C. Groen, L.A.A. Peffer, J.A. Moulijn, J. Pérez-Ramírez, Microporous Mesoporous Mater. 69 (2004) 29–34.
[29] J.C. Groen, J.A. Moulijn, J. Pérez-Ramírez, Microporous Mesoporous Mater. 87 (2005) 153–161.
[30] D. Tzoulaki, A. Jentys, J. Pérez-Ramírez, K. Egeblad, J. Lercher, Catal. Today 198 (2012) 3–11.
[31] M. Ogura, S. Shinomiya, J. Tateno, Y. Nara, M. Nomura, E. Kikuchi, M. Matsukata, Appl. Catal. A Gen. 219 (2001) 33–43.
[32] Q. Zhou, Y.Z. Wang, C. Tang, Y.H. Zhang, Polym. Degrad. Stab. 80 (2003) 23–30.
[33] L.L. Su, L. Liu, J.Q. Zhuang, H.X. Wang, Y.G. Li, W.J. Shen, Y.D. Xu, X.H. Bao, Catal. Lett. 91 (2003) 155–167.
[34] J.S. Jung, J.W. Park, G. Seo, Appl. Catal. A Gen. 288 (2005) 149–157.
[35] S. Gopalakrishnan, A. Zampieri, W. Schwieger, J. Catal. 260 (2008) 193–197.
[36] M. Bjørgen, F. Joensen, M.S. Holm, U. Olsbye, K.-P. Lillerud, S. Svelle, Appl. Catal. A Gen. 345 (2008) 43–50.
[37] Y.-Q. Song, Y.-L. Feng, F. Liu, Ch.-L. Kang, X.-L. Zhou, L.-Y. Xu, G.-X. Yu, J. Mol. Catal. 310 (2009) 130–137.
[38] H. Mochizuki, T. Yokoi, H. Imai, S. Namba, J.N. Kondo, T. Tatsumi, Appl. Catal. A Gen. 449 (2012) 188–197.
[39] X. Zhu, L.L. Lobban, R.G. Mallinson, D.E. Resasco, J. Catal. 271 (2010) 88–98.
[40] A.G. Gayubo, A. Alonso, B. Valle, A.T. Aguayo, J. Bilbao, Appl. Catal. B Environ. 97 (2010) 299–306.
[41] L. Zhao, J. Gao, C. Xu, B. Shen, Fuel Process. Technol. 92 (2011) 414–420.
[42] A.N.C. Van Laak, L. Zhang, A.N. Parvulescu, P.C.A. Bruijnincx, B.M. Weckhuysen, K.P. De Jong, P.E. De Jongh, Catal. Today 168 (2011) 48–56.
[43] Y. Gu, N. Cui, Q. Yu, C. Li, Q. Cui, Appl. Catal. A Gen. 429–430 (2012) 9–16.
[44] A.S. Oliveira, S.J.S. Vasconcelos, J.R. Sousa, F.F. Sousa, J.M. Filho, A.C. Oliveira, Chem. Eng. J. 168 (2011) 765–774.
[45] H. Atia, U. Armbruster, A. Martin, Appl. Catal. A Gen. 393 (2011) 331–339.
[46] L.G. Possato, R.N. Diniz, T. Garetto, S.H. Pulcinelli, C.V. Santilli, L. Martins, J. Catal. 300 (2013) 102–112.
[47] J.C. Groen, L.A.A. Peffer, J.A. Moulijn, J. Pérez-Ramírez, Chem. Eur. J. 11 (2005) 4983–4994.
[48] S. Brunauer, P.H. Emmet, E. Teller, J. Am. Chem. Soc. 60 (1938) 309–319.
[49] B.C. Lippens, J.H. de Boer, J. Catal. 4 (1965) 319–323.
[50] E.P. Barrett, L.G. Joyner, P.P. Halenda, J. Am. Chem. Soc. 73 (1951) 373–380.
[51] J.C. Groen, M.C. Doorn, L.A.A. Peffer, in: D.D. Do (Ed.), Adsorption Science and Technology, World Scientific, Singapore, 2000.
[52] C.A. Emeis, J. Catal. 141 (1993) 347–354.
[53] S.C. Fung, C.A. Querini, J. Catal. 138 (1992) 240–254.
[54] H. Chen, T. Sun, D. Sui, J. Dong, Anal. Chim. Acta 698 (2011) 27–35.
[55] M.L. Pisarello, B.O. Dalla Costa, N.S. Veizaga, C.A. Querini, Ind. Eng. Chem. Res. 49 (2010) 8935–8941.
[56] K.S.W. Sing, D.H. Everett, R.A.W. Haul, L. Moscou, R.A. Pierotti, J. Rouquerol, T. Siemieniewska, Pure Appl. Chem. 57 (1985) 603–619.
[57] V. Rac, V. Rakic, Z. Miladinovic, D. Stosic, A. Auroux, Thermochim. Acta 567 (2013) 73–78.
[58] F. Rouquerol, J. Rouquerol, K.S.W. Sing, in: F. Schüth, K.S.W. Sing, J. Weitkamp (Eds.), Handbook of Porous Materials, vol. 1, Wiley-VCH, Weinheim, 2002.
[59] B.C. Lippens, B.G. Linsen, J.H. de Boer, J. Catal. 3 (1964) 32–37.
[60] S. Mitchell, J. Pérez-Ramírez, Catal. Today 168 (2011) 28–37.
[61] R.M. Dessau, E.W. Valyocsik, N.H. Goeke, Zeolites 12 (1992) 776–779.
[62] G.L. Woolery, G.H. Kuehl, H.C. Timken, A.W. Chester, J.C. Vartuli, Zeolites 19 (1997) 288–296.
[63] D. Esquivel, A.J. Cruz-Cabeza, C. Jiménez-Sanchidrián, F.J. Romero-Salguero, Microporous Mesoporous Mater. 142 (2011) 672–679.
[64] V. Vishwanathan, K.-W. Jun, J.-W. Kim, H.-S. Roh, Appl. Catal. A Gen. 276 (2004) 251–255.
[65] A. Janin, M. Maache, J.C. Lavalley, J.F. Joly, F. Raatz, N. Szydlowsky, Zeolites 11 (1991) 391–396.
[66] G.L. Qin, L. Zheng, Y.M. Xie, C.C. Wu, J. Catal. 95 (1985) 609–612.
[67] B.L. Su, V. Norberg, Zeolites 19 (1997) 65–74.
[68] M.S. Holm, S. Svelle, F. Joensen, P. Beato, C.H. Christensen, S. Bordiga, M. Bjørgen, Appl. Catal. A Gen. 356 (2009) 23–30.
[69] T. Armaroli, A. Gutierrez Alejandre, M. Bevilacqua, M. Trombetta, F. Milella, J. Pérez-Ramírez, G. Busca, Stud. Surf. Sci. Catal. 135 (2001) 346.
[70] H.V. Brand, A. Redondo, P.J. Hay, J. Mol. Catal. A 121 (1997) 45–62.
[71] U. Fleischer, W. Kutzelnigg, A. Bleiber, J. Sauer, J. Am. Chem. Soc. 115 (1993) 7833–7838.
[72] J.P. Marques, I. Gener, P. Ayrault, J.C. Bordado, J.M. Lopes, F. Ramoa Ribeiro, M. Guisnet, Microporous Mesoporous Mater. 60 (2003) 251–262.
[73] M. Guisnet, P. Ayrault, C. Coutanceau, M.F. Alvarez, J. Chem. Soc. Faraday Trans. 93 (1997) 1661–1665.